Onboard flow visualization in a Pelton turbine bucket

Alexandre PERRIG*	EPFL-LMH, Switzerland	alexandre.perrig@epfl.ch
Mario VALLE	CSCS, Switzerland	mvalle@cscs.ch
Mohamed FARHAT	EPFL-LMH, Switzerland	mohamed.farhat@epfl.ch
Etienne PARKINSON	VATech SA, Switzerland	etienne.parkinson@vatech-hydro.ch
Jean FAVRE	CSCS, Switzerland	jfavre@cscs.ch
François AVELLAN	EPFL-LMH, Switzerland	francois.avellan@epfl.ch

Key words: Pelton turbine, bucket, flow, visualization, free-surface

Abstract

Flow visualizations using endoscopes in a 21-bucket single-injector reduced scale Pelton turbine are performed for 2 operating points. 2 types of visualizations are performed with a CMOS high-speed camera: (i) an onboard visualization of the flow in the bucket relative frame of reference; (ii) an external visualization technique in the absolute frame of reference. The flow observations evidence the unsteadiness of the successive steps of jet/bucket interaction, free surface flow development and evolution throughout the bucket duty cycle. The impact of the bucket cutout lips on the jet leads to significant perturbations of the free surface of the jet, inducing an outburst due to probable compressible effects. The front of the jet appears not to follow the bucket surface, but to overfly it and impinge later in the duty cycle. The cut jet remains attached to the bucket backside and disintegrates in several water threads. The end of the evacuation process evidences an important stratification of the flow, and a line of droplets is released from the cutout edges and the tip along the entire runner periphery due to the water saturated atmosphere prevailing in the casing.

Résumé

Une série d'observations de l'écoulement dans une turbine Pelton à 1 jet est menée à l'aide d'endoscopes pour 2 points de fonctionnement. 2 types de visualisations sont réalisés avec une caméra CMOS haute-vitesse: (i) observation embarquée de l'écoulement dans l'auget dans le repère relatif; (ii) observation externe depuis le repère absolu. Les résultats mettent en évidence le caractère instationnaire de l'interaction jet/auget, du développement et de l'évolution de l'écoulement à surface libre au cours de l'arc de travail de l'auget. L'impact des lèvres de l'échancrure sur la surface du jet génère d'importantes perturbations, ainsi qu'un éclatement dû à de probables effets compressibles. Le front du jet ne suit pas la courbure de la surface intérieure de l'auget, mais la survole et la percute plus tard dans l'arc de travail. La portion coupée du jet reste attachée au dos de l'auget et se fragmente en une série de filaments liquides. La fin du processus d'évacuation montre une stratification de l'écoulement, ainsi que la présence d'une ligne de gouttes d'eau s'échappant des augets par les bords de l'échancrure et la pointe, due à la saturation de l'atmosphère régnant dans le bâti.

Introduction

The flow in Pelton turbines has not been analyzed so far with such detail as the flow in the reaction turbines, and the understanding of the physics of the flow is weak. One of the reasons is that the flow patterns and the hydraulic losses are very difficult to observe and quantify: the flow processes include jets, spray formation, free surfaces and film flows, secondary flows, and complex interaction between the components. The fundamental unsteadiness of the flow makes the task even more difficult. As the surroundings of the turbine are contaminated with a large population of droplets of various sizes stemming from the water sheets break-up, the jet dispersion, and the water sheets collision with the casing walls, the atmosphere appears foggy, and the visibility is poor. Moreover, features of interest hide between the buckets, far from the casing walls, and are spread on a significant depth.
Thereby few experimental visualizations of the flow in Pelton turbines were performed so far, and most of them in simplified configurations. Guilbaud *et al.* (Ref 1) investigated the flow in a simplified 2*D* fixed bucket and Lowy (Ref 2) investigated particularly the interaction process of the jet by the bucket cutout in a fixed bucket. Bachman *et al.* (Ref 3) and Kvicinsky *et al.* (Ref 4) performed flow visualizations around rotating Pelton runners with conventional lenses protected from the splashes by tubes and lighted by stroboscopes.
To enable a close observation of the unsteadiness of the bucket flow, a visualization technique using medical endoscopes bound to a high-speed camera has been developed. A semi-continuous lighting system allows observing continuous flow sequences. The results obtained from 2 approaches are presented: (i) visualizations of the relative flow in a bucket with an onboard endoscope and (ii) external visualizations of the absolute flow.

Visualizations techniques

The experimental investigations are performed for a single-injector reduced scale Pelton turbine model, Fig.1, for 2 operating points, see Table 1. The specific energy is limited to 200 JKg^{-1} (20 *m* head) to reduce the rotational speed and thus the centrifugal load on the distal lens of the onboard endoscope and to get the most favorable conditions of observation by reducing the amount of splashing water.

Table 1 Case study characteristics.

OP	z_o	z_b	D_1/B_2	$\varphi_{B_2}/\varphi^{\wedge}_{B_2}$	$\psi_1/\psi^{\wedge}_1$
1	1	21	4.09	1.12	0.89
2				0.57	1.00

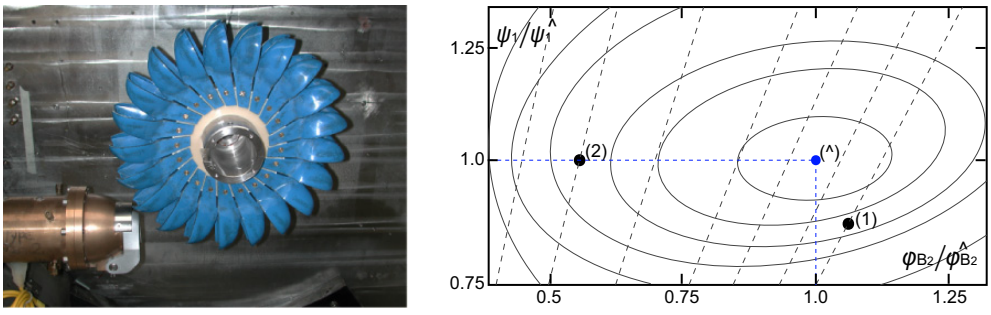

(*a*) Test runner (*b*) Investigated operating points

Figure 1 Test runner and operating points investigated.

Onboard visualization setup

A miniature endoscope, see Fig.2a, is located so that the distal lens is at the root of one half bucket. The advantages are: (i) no water is to be expected there during normal operation, as Pelton's modification to Knight's original impulse turbine was precisely to avoid water flowing towards the flange (Ref 5); (ii) the mounting is non-intrusive; (iii) the field of observation is not obstructed by the splitter; (iv) the radial acceleration prevents droplets to stick on the distal lens. An observation grid is drawn on the bucket inner surface, as schematized by Fig.2b. The

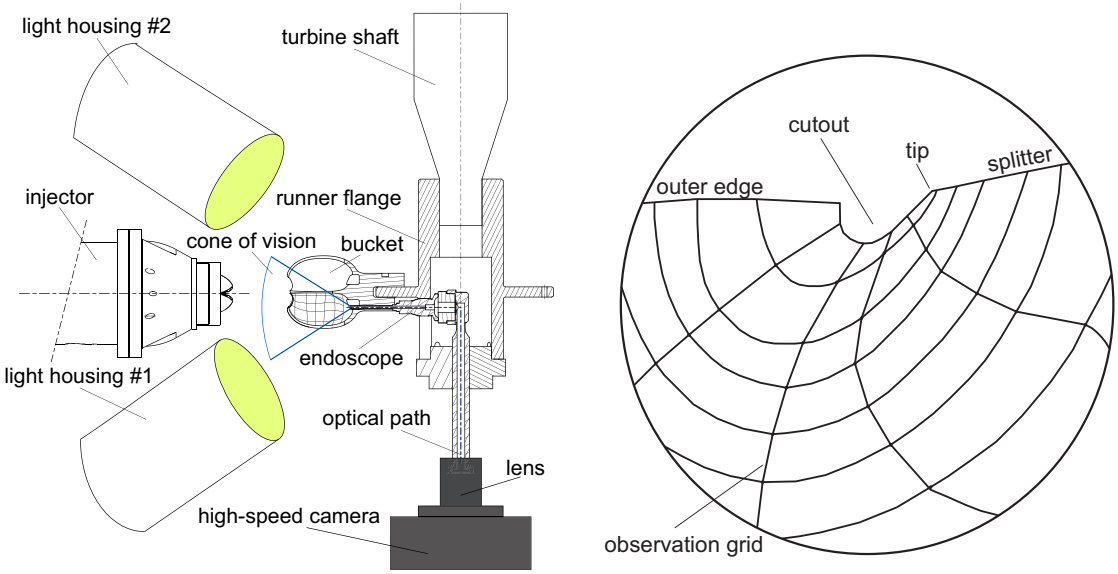

(*a*) Endoscope location (*b*) Area observed

Figure 2 Onboard endoscope location and field of view

CMOS camera head is kept outside the rotating parts of the test rig. The observation frames are transmitted via a 90° optical deflector passing through the runner rotation axis, and protruding outside the test rig window. The high-speed camera is mounted on a 4-degree-of-freedom adjustable support, allowing to align its lens with the deflector axis. The advantages of this setup are: (i) no data to transfer through slip rings; (ii) no electronic component in rotation; (iii) no mass unbalance. The flashlights are installed in waterproof housings that are mounted as close as achievable to the runner. An optical encoder is fitted on the 90° deflector, giving a +5 *V* TTL pulse at each runner rotation. The TTL signal is sent via an adjustable delay line unit set to trig the camera and the flash units synchronously at the desired runner angular position. The camera delay and flashlights jitter are short enough to be neglected. Even if the light source and camera capabilities allow measuring a complete bucket duty cycle, *i.e.* more than 90°, the non-moving assembly of the lighting system claims for a division of the duty cycle in overlapping subcycles to maintain adequate lighting conditions. Table 2 summarizes the experimental conditions.

Table 2 Experimental conditions.

shutter speed	frame rate	flash duration	resolution	frames per cycle	subcycles
μs	fps	ms	$pixels \times pixels$	–	–
6	6000	6	512×512	35	7

External flow visualizations setup

The onboard observations are completed by a series of visualizations carried on in the absolute frame of reference using a large endoscope. The endoscope ocular is bound to the same camera mounted on a light tripod. The distal lens of the endoscope is fitted with a pneumatic wiping system.

Images processing

The images captured by the onboard system suffer 2 major limitations: (i) the image contrast and luminosity vary depending on the bucket angular position; (ii) the field of view rotates as the endoscope rotates with the turbine rotor. A semi-automated process is set up to transform the raw images output by the camera into an improved quality sequence of images with a steady point of view. The image processing consists of 4 steps: (i) montage of the frames stemming from the subsequent subcycles; (ii) file names and formats adjustment, contrast and luminosity enhancement, and images de-rotation. This step is not sufficient to produce a steady image along the whole bucket duty cycle because of the mechanical precession of the optical deflector; (iii) the image center and viewing aperture of the endoscope on selected images in the sequence are marked; (iv) the collected positions are interpolated on the whole image sequence and used to re-center the endoscope view aperture and a mask is applied to remove the features external to the endoscope aperture.

Results

Angular datum definition

The duty cycle of any bucket *j* of the runner is defined as the arc out of bucket *j* rotation circle where it sees water transiting on its surface. The duty cycle ranges from the first encounter of bucket *j* tip with the upper generator of the jet to the evacuation of the last water particle stemming from the lower generator of the jet, *i.e.* arc *AB* on Fig.3. The exact angular position of points *A* and *B* are depending on the operating conditions. An univocal angular datum is hence needed. Bucket *j* datum is consequently set as the angular position where the position along bucket *j* splitter located on D_1 intersects the theoretical jet axis, as defined by Fig.3. The

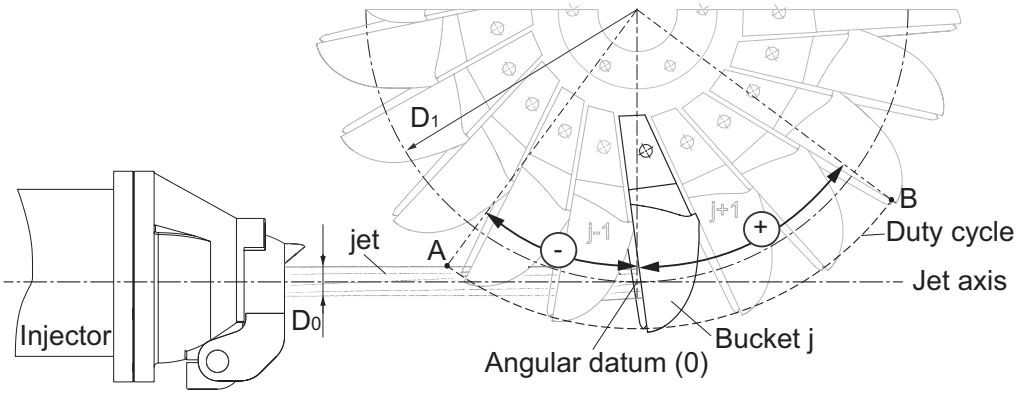

Figure 3 Bucket angular datum definition

angular positions of bucket *j* duty cycle preceding the datum are negative, while the the angular positions succeeding to the datum are positive.

Bucket flow sequence

The flow sequence of bucket j duty cycle is divided in 6 steps (Ref 3) (Ref 6). The description of the flow sequences is performed according to Fig.4 and 5 for the onboard relative observations for *OP*1 and *OP*2 respectively, and Fig.6 and 7 for the external observations, for *OP*1.

(i) Approach of the tip to the jet ($< -40°$).

Beside appearing striated and rippled, the jet surface exhibits perturbations along its upper generator, detail *a*, and a series of convected impact craters, detail *b*, Fig.6.

(ii) Initial feeding process. ($-40°$ - $-10°$).

Once the tip and the cutout lips backside are in contact with the jet upper surface, the jet starts to separate in 2 branches, *i.e.* the upper one, that flows in bucket j, and the lower one that continues to feed bucket $j + 1$. The image sequence show an outburst of the jet, and the appearance of a splay crown of water threads on the upper side, detail *c*, and a radial splashing water adhering to some extend to the ribs on the backside, detail *d*, animated by almost the same velocity as the jet. The jet front and the splay crown, detail *c*, fly over bucket j and impinges on it later in the cycle, at around $-17°$ for *OP*1 and $-23°$ for *OP*2. Immediately after the impact, the onset of foam, detail *e*, is clearly visible. At this point the jet is already partially cut by bucket $j - 1$. Thereafter, the flow evolves into the expected sheet flow, detail f, moving first slightly towards the root and then laterally towards the outer edge. The outflow process, detail *g*, starts at $\sim -10°$.

(iii) Entire separation of the jet ($-10°$ - $0°$).

At this point the impinging main flow feeds bucket j mainly normally to the splitter. The now entirely separated portion of the jet remains attached to bucket $j - 1$ backside far in the duty cycle, as predicted by Lowy (Ref 2) and observed by Bachmann (Ref 3). In addition, it seems to be deflected against bucket $j - 1$ backside. The deformations it displays match well the predictions made by Lowy (Ref 2): the cross-section of the jet is crescent-shaped, concave against bucket $j - 1$ backside. The cross-section consists of 2 different flows: the core, detail *h*, practically filled with liquid and the spray, which consists of numerous single separated water threads, detail *i*. The resulting section is much larger than the original jet diameter, and impinges not only on the splitter but also on the established water sheets, detail f. The water sheet for *OP*2 exhibits a tumescence, detail $f1$, that appears around $-13°$ and becomes larger at $-4°$.

(iv) Last stage of inflow ($0°$ - $15°$).

The last threads and droplets of the distorted and disintegrated end of the jet, detail *i*, enter bucket j partially on the bottom surface and partially on the lateral edges next to the cutout. Some of the water escapes bucket j directly through the cutout in a radial direction, detail *j*, even at very low discharge, see *OP*2, Fig.5.

(v) Last stage of outflow ($15°$ - $50°$).

The water sheet presents a corrugated surface at the end as it not fed anymore, detail *k*. The outflow sheet remains fully developed late in the duty cycle, and becomes thinner and thinner until it breaks up, detail *m*, at first near the root and then towards the front. The end of the outflow process shows a significant stratification of the flow: the sheet appears to slide film by film, detail *n*.

(vi) Series of droplets (-50° - ∞).
The outflow never comes to an end. A line of droplets, detail *l*, is visible along the entire runner periphery. The droplets are released from the outer edge tips, on the external side of the cutout, and from the splitter tip.

Flow analysis
The jet surface perturbations, detail *a* in Fig.6, are caused by the impact of droplets escaping bucket *j* from the splitter tip, detail *l*, and not by the blockage of a pocket of air as assumed by Bachmann (Ref 3). Only few droplets of small sizes are ejected radially and are moving with a fast decreasing velocity. They are therefore most unlikely to induce rain erosion damages on the buckets (Ref 7) (Ref 8). The series of convected craters, detail *b* on Fig.6, is caused by the impact of drops of larger size ($\simeq 3-5mm$). These droplets stem either from condensation on the test rig walls or from the bounce of splashing water on the injector body. The presence of such higher scale perturbations is likely to promote the occurrence of erosion damages on the cutout lips (Ref 7) (Ref 8).

Upon impact of the cutout, the jet surface bursts, and the cut section expands radially from the jet axis and forms a splay crown, detail *c* on Fig.4, 5 and 7. The conjunction of 2 phenomena explain the jet outburst: (i) the impact is likely to generate compression waves that are released across the free surface. Indeed, some studies (Ref 9) have shown that during the early stages of the impact of a rigid solid on a fluid, high compressive stresses are generated in the vicinity of the area of contact for times of the order of microseconds, followed by outward radial flow of liquid at high speed. (ii) The cutout lips form an obstacle that the flow has to go round, thus prolonging the normal to the jet velocity component generated by the impact. All sequences clearly indicate that the cut section of the jet does not follow bucket *j* surface, but overflies it due the bucket longitudinal curvature. The water threads forming the splay crown are caused by the cohesion forces between the water molecules and their backwards curved shape to their drag that is significantly higher than that of the smoother jet surface. In fact, the cutout lips appears to act like a spillway, inducing a significant aeration process in the jet front (Ref 10), as illustrated by Fig.8.

The radial splashing water, detail *d* on Fig.7, stems from the outburst of the jet at the moment of impact on the backside of bucket *j* cutout, and therefore has the same physical origin as the splay crown. A remarkable feature, however, appears in the images sequence displayed in Fig.(7): the flow adheres to some extend on bucket *j* ribs, before to separate with a significant lateral velocity component. The local curvature of the bucket ribs probably generates a so-called Coanda effect, forcing the flow to stick on it until the separation occurs (Ref 11) (Ref 12).

The jet front breaking on bucket *j* inner surface coincides with the onset of foam, detail *e* on Fig.4, which is due to the release of the air captured by the splay jet front, detail *c*. The presence of large amounts of air can promote local compressive effects. Indeed, the pressure peaks measured (Ref 4) and erosion damages observed (Ref 14) (Ref 7) coincide both in space and in time to the impact of the splay crown on bucket *j* surface.
The tumescence, detail $f1$ on Fig.5, observed for $OP2$ at -4°, is the probable sign of local mixing losses. It is likely to be caused by the encounter of 2 streams, both originating from the splitter and working against each other (Ref 2). One water filament flows towards the root, while the other is already moving towards the front.

The cut section adhesion to bucket $j-1$ backside is caused by the apparition of a zone of low pressure, due to the velocity of the jet greater than that of the bucket (Ref 3). The deflexion towards bucket $j-1$ backside may be induced by the bucket ribs curvature that promote the Coanda effect. The fragmentation in the liquid core, detail *h* and the threads *i*, see Fig.4 and 5, arise because the lateral edges of the separated jet have lost more kinetic energy than the core. The deflected jet is larger than the initial jet, and thus the outer filaments are splashing directly on the bottom surface of bucket *j*, guidance through the splitter being lost, generating further mixing losses. The phenomenon is well visible at around $+5^\circ$ for $OP1$ and $OP2$, Fig.4.

The cutout drain, detail *j* on Fig.4 and 5, is related to the spreading over of the water sheet, driven by the pressure increment across the jet towards the bucket face. This, in turn, generates a motion in the fluid across the the main flow direction perpendicularly to the bucket cross-section (Ref 13), causing the overflow through the cutout.

The water film stratification, detail *n* in Fig.5, appears as each film layer exhibits a slightly different trajectory, most probably due to the change in the balance of the inertia, surface tension and Coriolis forces across the boundary layer. In fact, as the velocity changes across the boundary layer, so does the Coriolis force.

The ejection of the series of droplets, detail *l* in Fig.4, 6 and Fig.7, is fed by the vapor-saturated atmosphere that prevail in the casing. The bucket surfaces act as a dew trap for the micro water droplets: the intersticial volume between the buckets is in depression due to the runner rotation. The droplets captured by the buckets then amalgamate until they form volumes of water heavy enough to be centrifuged.

Conclusion

The flow observation techniques presented in this paper provide a complete insight of the successive events throughout the duty cycle of one bucket of a single-injector Pelton runner from the relative frame of reference. The unsteadiness of the free surface flow in a Pelton turbine bucket is put into evidence.

As the jet has to flow across the contaminated atmosphere of the casing, its surface exhibits perturbations that can influence the flow in the buckets. Aside from insuring the cleanest flow out of the injector, the drop impact probability must be reduced, otherwise the most perfect bucket will not produce acceptable efficiencies. Moreover, too much protuberances on the jet promote erosion damages. In the case of multi-jet facilities the problem of the cutout drain is particulary detrimental, causing the so-called 'Falaise effect'.

The jet cut process displays more complexity than thought so far. It shows that compressible effects probably arise at the moment of initial contact, triggering the outburst of the jet that influences considerably the subsequent steps of the flow patterns on either sides of the bucket. Moreover, the onboard sequences show that the cut of the jet should be as neat as achievable, so that every filament of fluid impinges on the splitter in a favorable fashion. The shredded cut observed leads to considerable mixing losses.

Thereafter, the physical properties of water and more particularly of the free surface and surface tension play a significant role in the phenomena observed: they directly influence the shape of

the splay crown, the cut jet enlargement and deformation, the spray formation, and its fragmentation in water threads. The outflow process is also dependent on the balance between inertia, inter-molecular cohesion and friction forces.

Geometric characteristics of the the whole bucket, *i.e.* including the ribs and external surfaces, appear to have an influence on the flow, as they can generate Coanda effect and thus induce deviations of the water filaments far from their intended trajectories, what increases the losses either by lost kinetic energy or by mixing. It must be emphasized that geometric requirements are sometimes antinomic: for instance the cutout should be wide enough to prevent the series of droplets to impinge on the jet, but small enough to inhibit the cutout drain.

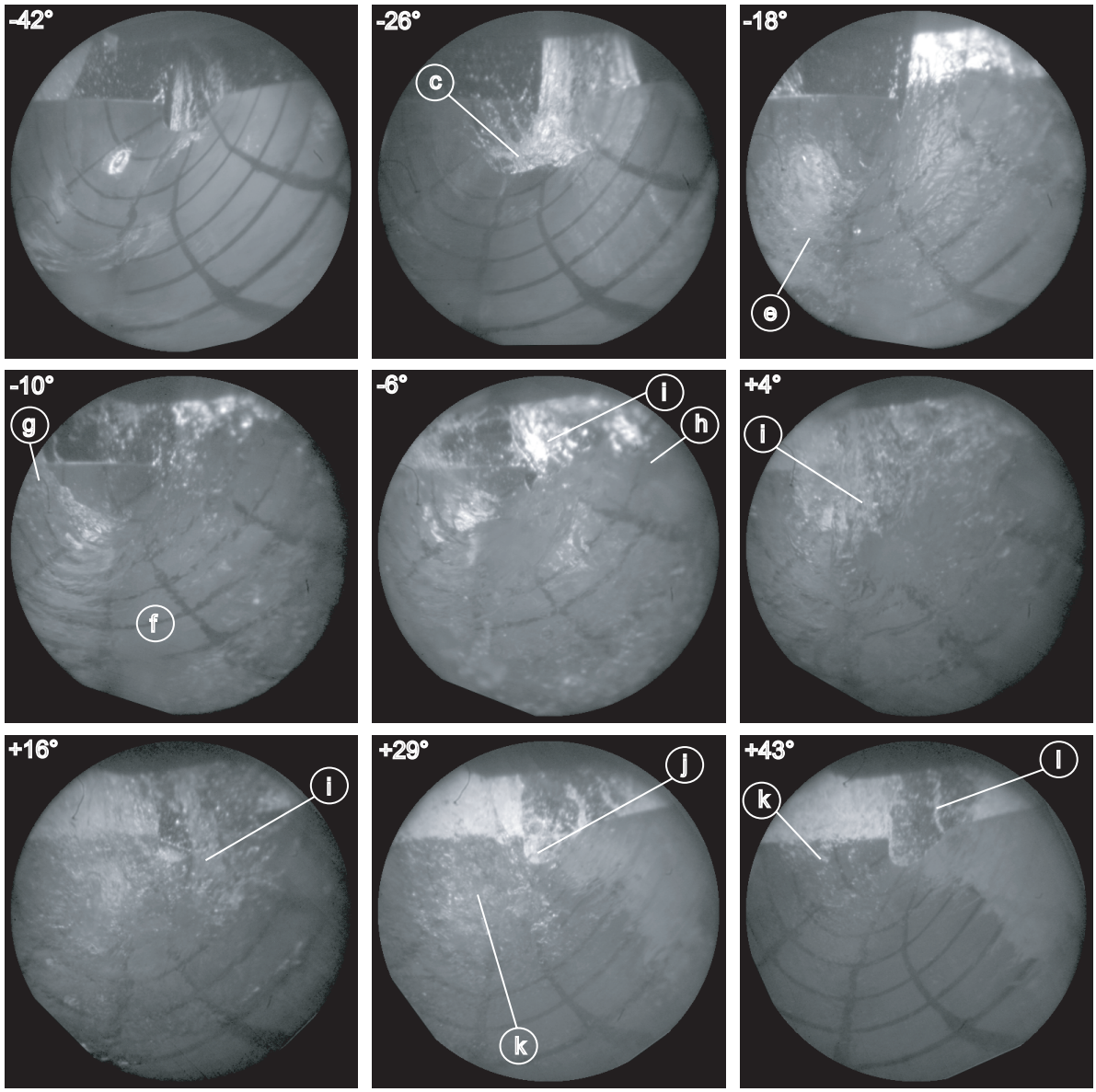

Figure 4 Bucket onboard film sequence, OP 1

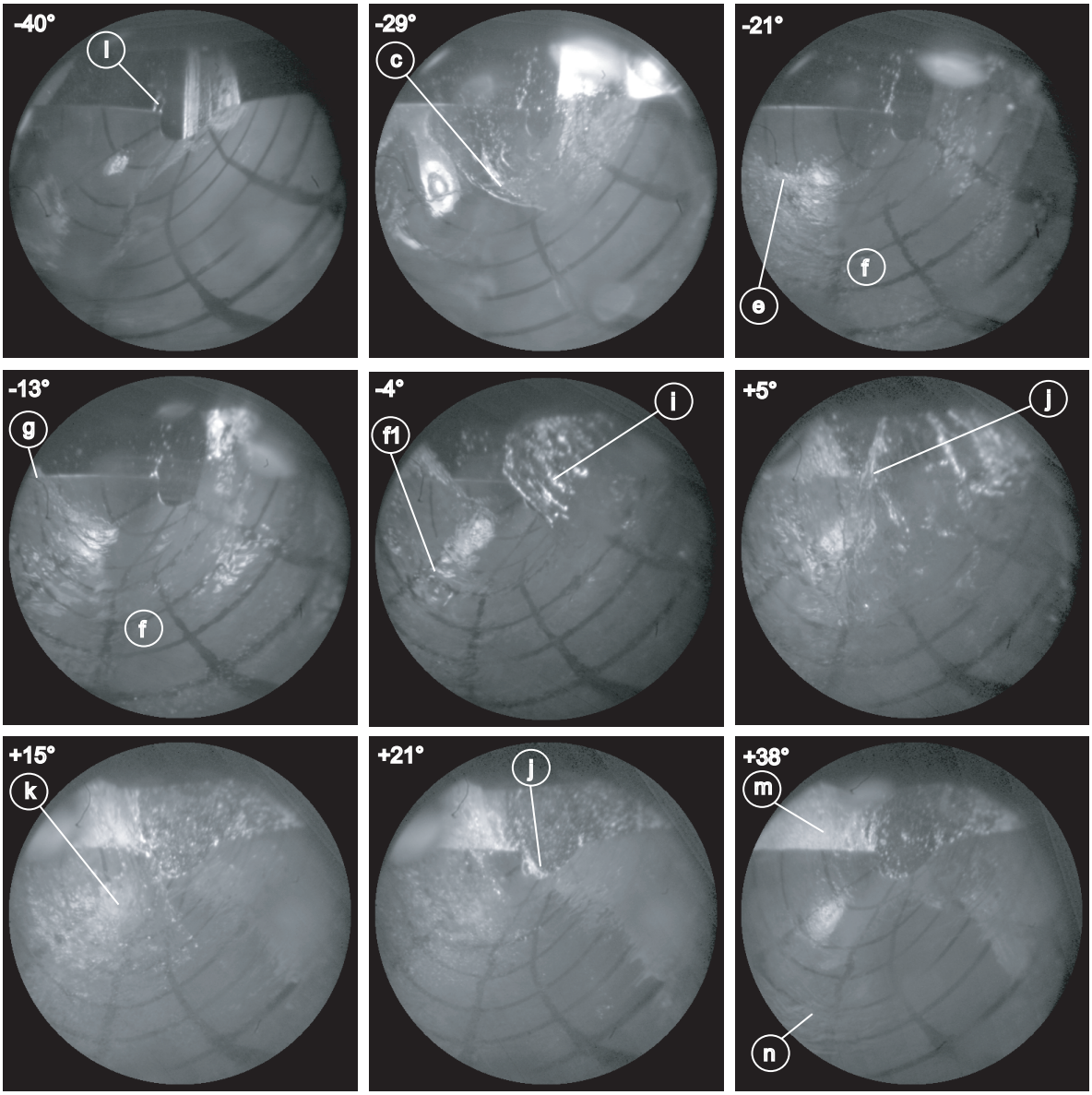

Figure 5 Bucket onboard film sequence, OP 2

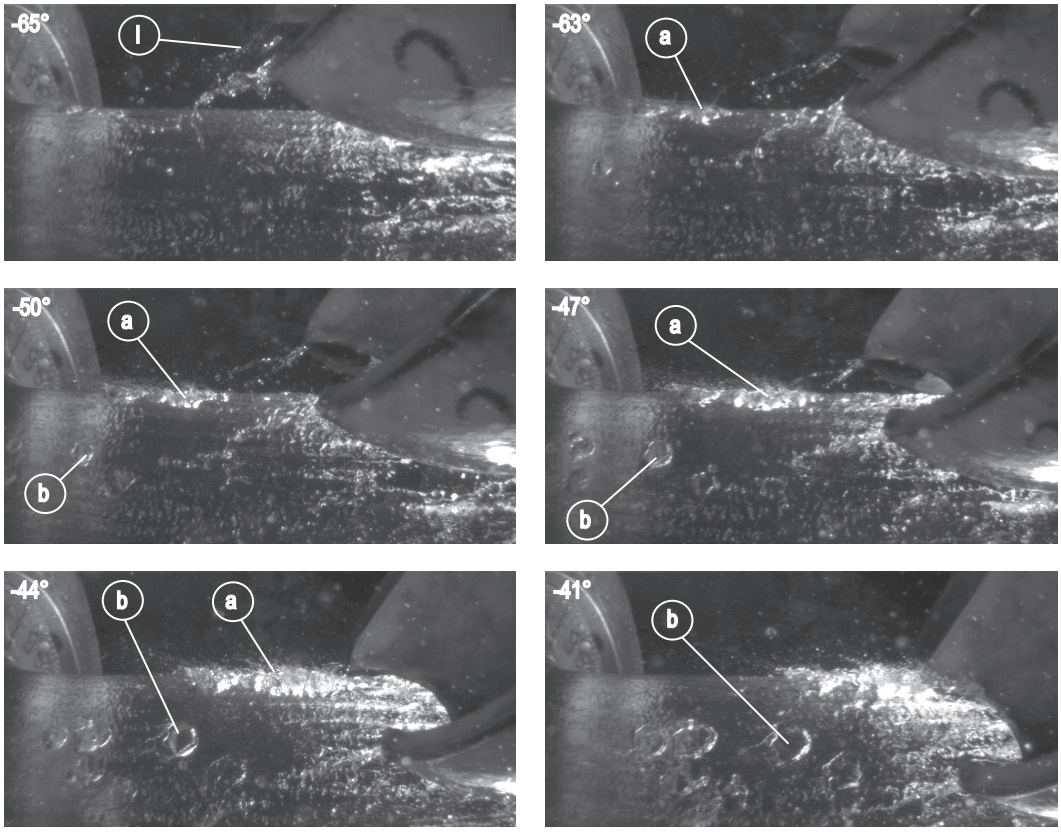

Figure 6 Jet surface perturbation by droplets impact, OP 1

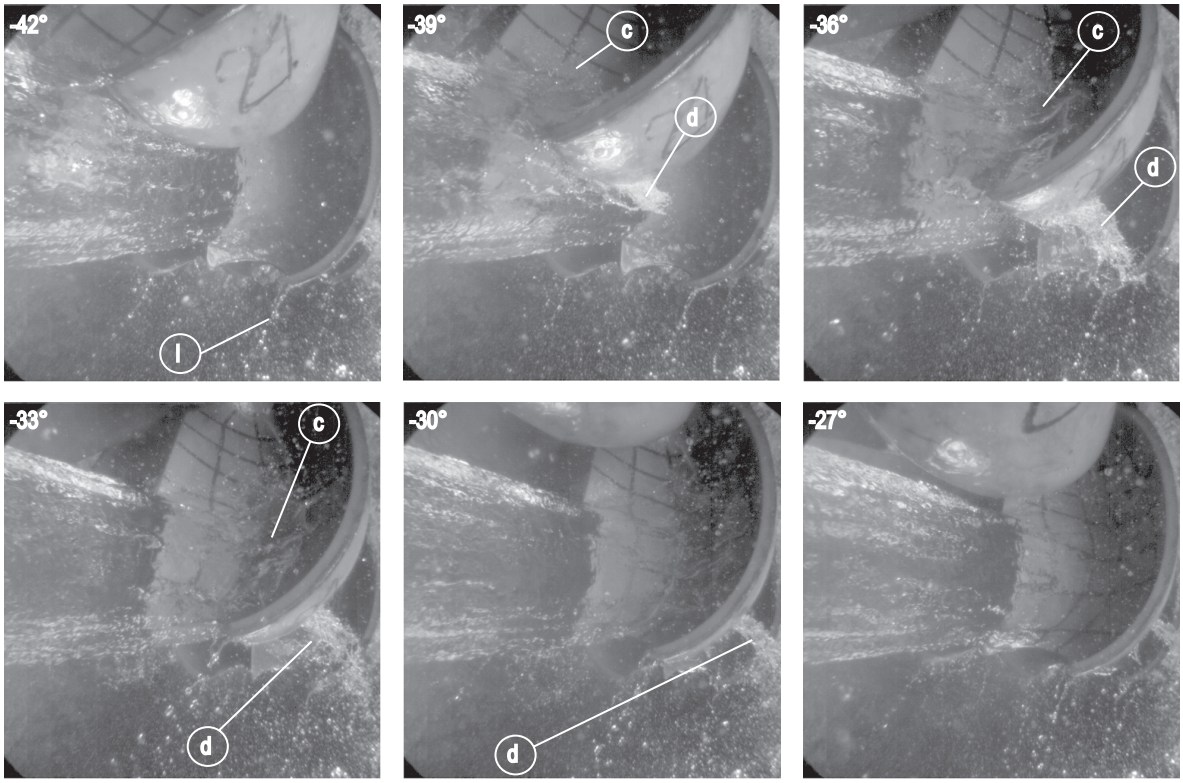

Figure 7 Bucket external observation, OP 1

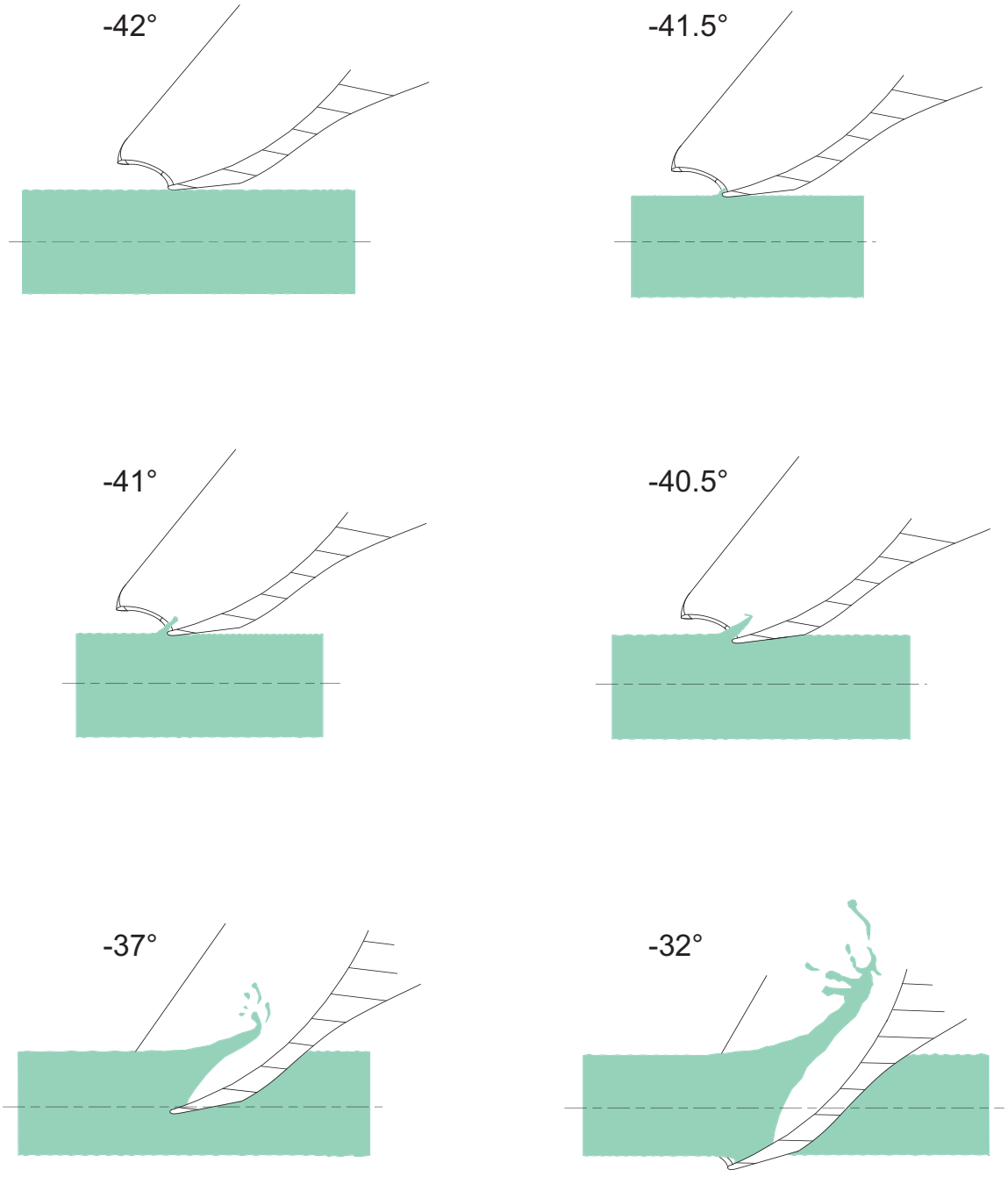

Figure 8 Interpretation of the spillway effect during the jet cut

Nomenclature

B_2	Bucket width $[m]$
D_1	Jet pitch circle diameter $[m]$
H	Test head $[m]$
Q	Discharge $[m^3 s^{-1}]$
z_o	Number of injectors $[-]$
z_b	Number of buckets $[-]$
ϕ_{B_2}	Discharge coefficient $[-]$: $\phi_{B_2} = \frac{Q}{z_o(\pi B_2^2/4)U_1}$
ψ_1	Energy coefficient $[-]$: $\psi_1 = \frac{2E}{U_1^2}$

Acknowledgements

The authors would like to thank the staff members of EPFL-Laboratory for Hydraulic Machines in Lausanne and of VATECH Hydro SA in Vevey, for their outstanding support. They would like to especially thank Mr. Bezençon, workshop head of the LMH and Mr. Pérusset, test rig engineer at VATech Hydro SA, for their dedication and enthusiastic support. This work is financially supported by the swiss promotion agency for innovation, KTI-CTI, Grant No. 6139.2, and VATECH Hydro SA.

References

Ref 1 Guilbaud, M., Houdeline, J.B., Philibert, R., Study of the flow in the various sections of a Pelton turbine, Proceedings of 15th IAHR Symposium on Hydraulic Machinery and Cavitation, São Paulo, Brazil, 1992, pp. 819-831.

Ref 2 Lowy, R., Efficiency analysis of Pelton wheels, Transactions of the ASME, vol.66, New York, August 1944, pp. 527-538.

Ref 3 Bachmann P., Schrer Ch., Staubli T., Vullioud G., Experimental flow studies on a 1-jet model turbine Pelton, Proceedings of 15th IAHR Symposium on Modern Technology in Hydraulic Energy Production, Belgrade, Yugoslavia, September 11-14, 1990, pp. 1-13.

Ref 4 Kvicinsky, S., Kueny, J.-L., Avellan, F., Parkinson, E., Experimental and numerical analysis of free-surface flows in a rotating bucket, Proceedings of 21th IAHR Symposium on Hydraulic Machinery and Systems, Lauanne, Switzerland, September 9-12, 2002, pp. 359-364.

Ref 5 Doble, W.A., The Tangential Water Wheel, Transactions of the American Institute of Mining Engineers, Vol.29, 1899, pp.1-42.

Ref 6 Perrig, A., Farhat, M., Avellan, F., Parkinson, E., Garcin, H., Bissel, C., Valle, M., Favre, J., Numerical flow analysis in a Pelton turbine bucket, Proceedings of 22nd IAHR Symposium on Hydraulic Machinery and Systems, Stockholm, Sweeden, June 29-July2, 2002, pp.A-10-3-1-14.

Ref 7 Grein, H., Cavitation pitting and rain erosion on Pelton runners, Proceedings of 15th IAHR Symposium on Modern Technology in Hydraulic Energy Production, Belgrade, Yugoslavia, September 11-14, 1990, pp. 1-9.

Ref 8 Engel, O.G., Damage produced by high-speed liquid-drop impact, J. Appl. Phys., vol.44, No.2, February 1973, pp.692-704.

Ref 9 Skalak, R., Feit, D., Impact on the surface of a compressible fluid, Trans. ASME, J. Eng. for Industry, vol. 88, August 1966, pp. 325-331.

Ref 10 Chanson, H., Air bubble entrainment in turbulent water jets discharging into the atmosphere, Transactions of the Australian civil/strucural Enginerring, vol. CE39, n^o 1, 1996, pp. 39-48.

Ref 11 Perrig, A., Avellan, F., Kueny, J.-L., Farhat, M., Parkinson, E., Flow in a Pelton Turbine Bucket: Numerical and Experimental Investigations, Journal of Fluids Engineering, vol. 128, Issue 2, pp. 350-358.

Ref 12 Wille, R., Fernholz, H., Report on the first european mechanics colloqium on the Coanda effect, J. Fluid Mech., vol.23, pp.801-819.

Ref 13 Raabe, J., The negative efficiency scale effect in Pelton turbines and its causes, Proceedings of 15th IAHR Symposium on Modern Technology in Hydraulic Energy Production, Tokyo, Japan, September 11-14, 1980, pp. 689-702.

Ref 14 Brivio, R., Zappi, O., La cavitazione nelle turbine Pelton (Parte II), L'energia elettrica, vol.73, No.4, Luglio-Agosto 1995, pp.266-270.